

The lattice QCD phase diagram in and away from the strong coupling limit

Ph. de Forcrand,^{1,2} J. Langelage,² O. Philipsen,³ and W. Unger³

¹*CERN, Physics Department, TH Unit, CH-1211 Geneva 23, Switzerland*

²*Institut für Theoretische Physik, ETH Zürich, CH-8093 Zürich, Switzerland*

³*Institut für Theoretische Physik, Goethe-Universität Frankfurt, 60438 Frankfurt am Main, Germany*

(Dated: May 13, 2018)

We study lattice QCD with four flavors of staggered quarks. In the limit of infinite gauge coupling, “dual” variables can be introduced, which render the finite-density sign problem mild and allow a full determination of the $\mu - T$ phase diagram by Monte Carlo simulations, also in the chiral limit. However, the continuum limit coincides with the weak coupling limit. We propose a strong-coupling expansion approach towards the continuum limit. We show first results, including the phase diagram and its chiral critical point, from this expansion truncated to next-to-leading order.

PACS numbers: 12.38.Gc, 13.75.Cs, 21.10.Dr, 21.65.-f

The properties of QCD as a function of temperature T and matter density are summarized by its phase diagram, whose determination is a major goal of large-scale heavy-ion experiments. Although the quark-gluon plasma has been observed at high temperature, further features of the phase diagram, especially a possible QCD critical point, have not been identified yet. On the theory side, heroic efforts have been devoted to numerical lattice simulations, which are the appropriate tool for non-perturbative phenomena like phase transitions. However, the fermion determinant becomes complex upon turning on a chemical potential μ coupled to the quark (or baryon) number. This so-called “sign problem” requires prohibitively large computer resources growing exponentially with the lattice 4-volume. Approaches to circumvent this problem are applicable when $\mu/T \lesssim 1$ only [1], and results on the QCD critical point are inconclusive. We want to make progress on this problem by means of a strong coupling expansion, as applied to zero density in the early days of lattice gauge theory or recently to finite temperature and density with heavy quarks [2, 3]. Here we want to address the opposite, chiral limit with a different strategy [4, 5]. Note that both for heavy and chiral quarks, the strong coupling approach gives access also to the cold and dense regime of nuclear matter [3, 6].

The sign problem occurs when elements $\langle \psi_i | \exp(-\delta\tau H) | \psi_j \rangle$ of the transfer matrix between states $|\psi_i\rangle$ and $|\psi_j\rangle$ sampled by Monte Carlo become negative. This problem is representation-dependent: if we could work in an eigenbasis of the Hamiltonian, all matrix elements would be non-negative. Thus, the sign problem will become milder if we can express the partition function in terms of approximate eigenstates. Now, we know that QCD eigenstates are color singlets. Therefore, instead of performing Monte Carlo on colored gauge links, as done in the usual approach where fermion fields are integrated out, we integrate the gauge links *first*, and work with the resulting color singlets. This strategy becomes particularly practical in the strong coupling limit, as we explain below. In this

regime, we reexpress the partition function as a sum over configurations of hadron worldlines, similar to the “dual variables” used in [7]. The resulting sign problem is extremely mild, which allows us to simulate large lattices at arbitrarily large chemical potentials, and reliably obtain the full QCD phase diagram. Of course, in the strong coupling limit $g \rightarrow \infty, \beta = 2N_c/g^2 \rightarrow 0$ (for N_c colors), the lattice is maximally coarse, whereas the continuum limit coincides with the weak coupling limit $g \rightarrow 0, \beta \rightarrow \infty$. In this letter, we first summarize and clarify the $\beta = 0$ phase diagram and then explain how to include the first, $\mathcal{O}(\beta)$ corrections, which allows us to measure Wilson loops at $\beta = 0$ and fermionic observables at $\mathcal{O}(\beta)$. We then present the QCD phase diagram for small $\beta > 0$. For $\mu = 0$ where we can crosscheck with the full Monte Carlo approach, perfect agreement is found for small β .

We adopt the staggered fermion discretization and the Wilson plaquette action with the partition function:

$$Z_{\text{QCD}} = \int d\psi d\bar{\psi} dU e^{S_G + S_F}, \quad S_G = \frac{\beta}{2N_c} \sum_P \text{tr}[U_P + U_P^\dagger] \quad (1)$$
$$S_F = am_q \sum_x \bar{\psi}_x \psi_x + \frac{1}{2} \sum_{x,\nu} \eta_\nu(x) \gamma^{\delta_{\nu 0}} \times [\bar{\psi}_x e^{a_t \mu \delta_{\nu 0}} U_\nu(x) \psi_{x+\hat{\nu}} - \bar{\psi}_{x+\hat{\nu}} e^{-a_t \mu \delta_{\nu 0}} U_\nu^\dagger(x) \psi_x] \quad (2)$$

with a and a_t the spatial and temporal lattice spacings, γ the anisotropy by which one may tune a/a_t , m_q the quark mass and μ the quark chemical potential (the baryon chemical potential is $\mu_B = N_c \mu$). The η 's are the usual ± 1 staggered phases. In the continuum limit $g \rightarrow 0$, our action describes QCD with 4 mass-degenerate quark species. In the opposite, strong coupling limit $g \rightarrow \infty$, the plaquette, 4-link coupling β vanishes and so does the gauge action S_G . Then, the integration over the links $U_\nu(x)$ factorizes into a product of one-link integrals which can be carried out analytically [8]. Finally, one performs the Grassmann integration over the fermion fields $\psi(x), \bar{\psi}(x)$, and obtains the partition function in terms of color-singlet, hadronic degrees of freedom (mesons and

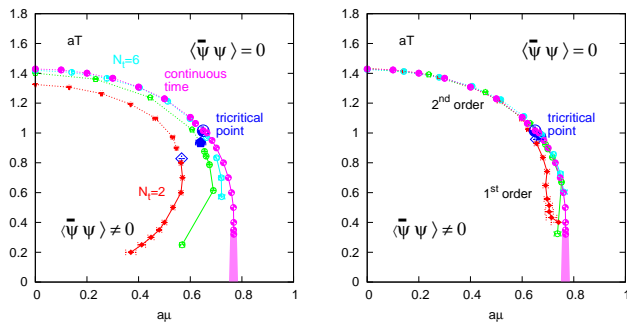


FIG. 1: *Left:* Lattice QCD phase diagram in the strong coupling limit, setting $a/a_t = \gamma^2$ following mean-field. Different results are obtained for different numbers N_t of time-slices: $N_t = 2$, $N_t = 4$ [6], $N_t = 6$ and $N_t = \infty$ (i.e. continuous Euclidean time) [17]. *Right:* Same, with corrected anisotropy $a/a_t = \gamma^2 \exp(c/\gamma^2)$ and $\mathcal{O}(1/N_t)$ corrections. All results coincide. The re-entrance at low aT is a finite- N_t artifact.

baryons) [4], as a sum over discrete graphs on the lattice:

$$Z_{SC} = \sum_{\{n,k,\ell\}} \prod_x w_x \prod_b w_b \prod_\ell w_\ell \quad (3)$$

$$w_x = \frac{N_c!}{n_x!} (2am_q)^{n_x}; \quad w_b = \frac{(N_c - k_b)!}{N_c! k_b!}. \quad (4)$$

The mesons are represented by monomers $n_x \in \{0, \dots, N_c\}$ on sites x and dimers $k_b \in \{0, \dots, N_c\}$ on bonds $b = (x, \hat{\nu})$, whereas the baryons are represented by oriented self-avoiding loops ℓ . The weight w_ℓ of a baryonic loop ℓ and its sign depend on the loop geometry [15]. Configurations $\{n, k, \ell\}$ must satisfy at each site x the constraint inherited from Grassmann integration:

$$n_x + \sum_{\hat{\nu}=\pm\hat{0},\dots,\pm\hat{d}} \left(k_{\hat{\nu}}(x) + \frac{N_c}{2} |\ell_{\hat{\nu}}(x)| \right) = N_c. \quad (5)$$

Due to this constraint, mesonic degrees of freedom (monomers and dimers) cannot occupy baryonic sites.

This system has been studied since decades, both via mean field [9–14] and by Monte Carlo methods [5, 6, 15]. In recent years, the latter have undergone a revival using the Worm algorithm [6, 16, 17], which violates the Grassmann constraint in order to sample the monomer two-point function $G(x, y)$, from which the chiral susceptibility can be obtained. These techniques have been applied to obtain all lattice data presented here. We study the chiral limit $m_q = 0$ which does not incur a penalty in computer cost, contrary to the usual determinantal approach. The staggered action S_F Eq. (2) then satisfies a $U(1)$ “remnant” chiral symmetry, which is spontaneously broken at low temperature and density, with order parameter $\langle \bar{\psi} \psi \rangle$. In Fig. 1 left, we show the (μ, T) phase diagram in the strong-coupling (SC) limit. It is qualitatively similar to the expected phase diagram of QCD in the chiral limit: the transition is of second order from $a\mu = 0$ up to a tricritical point $(a\mu_T, aT_T)$, then

turns first order. At finite quark mass, the second order line turns into a crossover and the tricritical point into a second order critical endpoint. Note the different phase boundaries obtained from lattices with different numbers N_t of time-slices: they converge to the continuous-time phase boundary as $N_t \rightarrow \infty$. But the N_t -dependence is strong, and there are indications of re-entrance at low temperature, supported by mean-field calculations [13], which only disappear in the continuous-time limit. There are two reasons for this: (i) the transition temperature is subject to $\mathcal{O}(1/N_t)$ corrections, as studied in [17]; (ii) temperatures $aT > 1/2$ can only be explored by using anisotropic lattices where $a/a_t > 1$. But the relationship between the bare anisotropy γ in the action S_F Eq.(2) and a/a_t is not known exactly. Mean-field indicates $a/a_t = \gamma^2$, which was used to obtain Fig. 1 left. Assuming the form $a/a_t = \gamma^2 \exp(c/\gamma^2)$ and allowing for small $\mathcal{O}(1/N_t)$ corrections (Fig. 1 right) produces much more consistent results.

A crucial question is whether this phase diagram develops qualitatively new features as β is increased from 0 to ∞ . At low temperature especially, things may change: when $\beta=0$, the transition at $\mu_c(T=0)$ separates a chirally-broken, baryon-free vacuum and a chirally-symmetric, baryon-saturated state with one static baryon per lattice site. That is a very crude cartoon of a nuclear matter phase: in the continuum limit, depending on the chemical potential, it may evolve into a nuclear liquid, a crystalline phase, a color superconductor, etc... A first insight may be gained by considering $\mathcal{O}(\beta)$ corrections to the $\beta=0$ phase diagram. At the same time, we can also address an interesting quantitative issue: the ratio $T_c(\mu=0)/\mu_c(T=0)$ is about $(160 \text{ MeV})/(300 \text{ MeV}) \sim 0.53$ in nature, but about $1.402/0.75 \approx 1.87$ when $\beta=0$. How does it vary with β ?

Corrections to the Strong Coupling Limit - To go beyond the strong coupling limit, a systematic expansion of the QCD partition function in β is needed, which we perform to first order $\mathcal{O}(\beta)$. Writing the $\beta=0$ partition function as $Z_{SC} = \int d\psi d\bar{\psi} Z_F$, with $Z_F(\psi, \bar{\psi}) = \int dU e^{S_F}$ the fermionic partition function, the $\beta \neq 0$ partition function Eq. 1 becomes:

$$Z_{\text{QCD}} = \int d\psi d\bar{\psi} dU e^{S_F + S_G} = \int d\psi d\bar{\psi} Z_F \langle e^{S_G} \rangle_{Z_F}, \quad (6)$$

$$\langle e^{S_G} \rangle_{Z_F} \simeq 1 + \langle S_G \rangle_{Z_F} = 1 + \frac{\beta}{2N_c} \sum_P \langle \text{tr}[U_P + U_P^\dagger] \rangle_{Z_F}, \quad (7)$$

where Eq. (7) is an $\mathcal{O}(\beta)$ truncation. We thus need the expectation value of the elementary plaquette $\text{tr}[U_P]$ in the strong coupling ensemble Z_F . The plaquette is composed of 4 links representing gluons, which provide new possibilities to make color singlets together with $\bar{\psi}_x \psi_{x \pm \hat{\mu}}$ propagating fermions.

This gives rise (for $N_c = 3$) to 19 terms, which are computed from the product $P = J_{ij} J_{jk} J_{kl} J_{li}$ of the one-

link integrals $J_{ij} \equiv \int dUU_{ij} \exp(\bar{\psi}U\phi - \bar{\phi}U^\dagger\psi)$ around an elementary plaquette [18–20] :

$$J_{ij} = -\sum_{k=1}^3 \frac{(3-k)!}{3!(k-1)!} [M_\psi M_\phi]^{k-1} \bar{\phi}_j \psi_i + \frac{1}{12} \varepsilon_{ii_2 i_3} \varepsilon_{jj_2 j_3} \bar{\psi}_{i_2} \phi_{j_2} \bar{\psi}_{i_3} \phi_{j_3} - \frac{1}{3} \bar{B}_\psi B_\phi \bar{\phi}_j \psi_i, \quad (8)$$

where M and B represent mesons and baryons. The first term describes the propagation of a $(\bar{q}g)$ anti-quark+gluon together with 0 to 2 mesons; the second term describes a (qqg) ; the third term is again a $(\bar{q}g)$ together with a baryon. From these, we compute the weight associated with a plaquette (or any Wilson loop) source term in the strong coupling configuration.

At the corners of the plaquette, the Grassmann variables ψ, ϕ are bound into baryons and mesons to fulfill the Grassmann constraint Eq.(5), giving rise to the 19 subgraphs mentioned above. Introducing a variable $q_P \in \{0, 1\}$ to mark the "excited" plaquettes P associated with the second term of Eq.(7), and corresponding variables q_b and $q_x = q_P$ for the links and the corners of such plaquettes, we can write the $\mathcal{O}(\beta)$ partition function in the same form as Eq.(3) with modified weights \hat{w} :

$$Z(\beta) = \sum_{\{n, k, \ell, q_P\}} \prod_x \hat{w}_x \prod_b \hat{w}_b \prod_\ell \hat{w}_\ell \prod_P \hat{w}_P \quad (9)$$

$$\hat{w}_x = w_x v_x, \quad \hat{w}_b = w_b k_b^{q_b}, \quad (10)$$

$$\hat{w}_\ell = w_\ell \prod_{\ell} w_{B_i}(\ell), \quad \hat{w}_P = \left(\frac{\beta}{2N_c}\right)^{q_P}, \quad (11)$$

where $v_x = (N_c - 1)!$ if x is the corner of an excited plaquette attached to an external meson line, $N_c!$ if it is attached to an external baryon line, 1 otherwise. Likewise, the weight of each baryon loop segment ℓ is modified by a factor $w_{B_1} = \frac{1}{(N_c-1)!}$, $w_{B_2} = (N_c - 1)!$, where B_1 and B_2 correspond to the second/third expression in Eq.(8). We can sample this partition function by the same worm algorithm as for $\beta = 0$, adding a Metropolis step to update the plaquette variables q_P . In practice, we found it simpler to obtain gauge observables via reweighting from the $\beta = 0$ ensemble.

Several qualitatively new features are made possible by including $\mathcal{O}(\beta)$ contributions: (i) the constituent quarks of baryons and mesons can now separate: hadrons are no longer point-like, but acquire a size $\sim a$; (ii) the baryon-baryon interaction can now proceed by quark exchange: it is no longer limited to the on-site Pauli exclusion principle; (iii) baryon saturation can now coexist with monomers, making chiral symmetry breaking possible in the dense phase similar to nuclear matter.

Wilson loops at $\beta = 0$ - Figs. 2 and 3 illustrate the dependence of the Polyakov loop and of the plaquette (time-like and space-like) on the chemical potential μ and the temperature T , at $\beta = 0$. The x -axis represents the

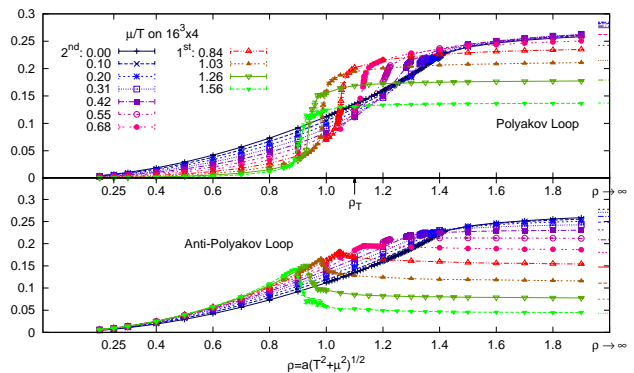


FIG. 2: Polyakov loop $\frac{1}{3} \langle \text{tr} L \rangle$ and anti-Polyakov loop $\frac{1}{3} \langle \text{tr} L^* \rangle$ as a function of (μ, T) on a $16^3 \times 4$ lattice at $\beta = 0$. The colors label successive values of μ/T , and the x -axis is $\rho \equiv a\sqrt{\mu^2 + T^2}$. At the tricritical point, $\rho_T = 1.10(2)$.

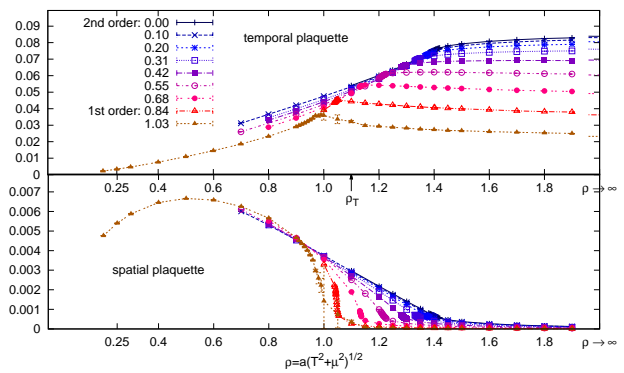


FIG. 3: Average spatial/temporal plaquette $\frac{1}{3} \langle \text{tr} P_s \rangle$, $\frac{1}{3} \langle \text{tr} P_t \rangle$ as a function of (μ, T) on a $16^3 \times 4$ lattice at $\beta = 0$. Wilson loops are sensitive to the chiral transition and develop a discontinuity as the transition turns first order. $\langle \text{tr} P_s \rangle$ varies oppositely to $\langle \text{tr} P_t \rangle$, and remains very small.

"distance" $a\sqrt{\mu^2 + T^2}$ from the vacuum, and different symbols are used for different values of μ/T . Several features are noticeable: (i) the plaquette has a non-zero value, even at $T = \mu = 0$. This is caused by the ordering effect of the fermions. Indeed, increasing the number of quark fields from 1 to 13 triggers restoration of the chiral symmetry [21]. (ii) The first-order phase transition is visible at large μ/T through a discontinuity in all Wilson loops, although it is associated with breaking/restoration of the chiral symmetry. This can be assigned to the non-zero latent heat. (iii) Even in the regime of small μ/T , where the chiral transition is second-order, the Polyakov loop is clearly sensitive to the transition as already found in $U(3)$ gauge theory [22], and reflecting the "entanglement" of confinement and chiral symmetry breaking seen in effective models [23].

Phase Diagram as a Function of β - We now show how to obtain the derivative $d(aT_c)/d\beta$ of the chiral transition temperature aT_c with respect to β . Since the worm algorithm samples the 2-point correlation function

$G(x_1, x_2)$, we can measure its integral, which is equal to the chiral susceptibility χ (there is no disconnected piece $\langle \bar{\psi}\psi \rangle^2$: since we set $m_q = 0$ and work in a finite volume, $\langle \bar{\psi}\psi \rangle = 0$ both in the chirally symmetric and broken phase),

$$\chi \equiv \langle (\bar{\psi}\psi)^2 \rangle = \frac{1}{L^3 N_\tau} \sum_{x_1, x_2} G(x_1, x_2). \quad (12)$$

At $\beta = 0$ and for some $\mu < \mu_T$, the critical temperature $aT_c(\mu)$ can be obtained from finite-size scaling: the curves $\chi(aT, L)L^{-\gamma/\nu}$ obtained on several lattice sizes L all intersect at $T = T_c(\mu)$, with a slope $\propto L^{1/\nu}$ at the intersection, as illustrated Fig. 4 left. The transition is in the $3d$ $O(2)$ universality class with known critical exponents, which facilitates the analysis. In the region of a first-order transition, $\mu > \mu_T$, this ansatz is modified accordingly, following Ref. [24]. When we turn on β , the chiral susceptibility changes, and we can easily measure its derivative, since

$$\frac{d\chi}{d\beta} = 3L^3 N_\tau \langle (\bar{\psi}\psi)^2 P_t \rangle - \langle (\bar{\psi}\psi)^2 \rangle \langle P_t \rangle. \quad (13)$$

While both the temporal and the spatial plaquettes formally enter in this expression, the latter is a factor $\gtrsim 10$ smaller than the former, cf. Fig. 3. The effect of β , to linear order, is illustrated Fig. 4 right. At temperature aT_c , the rescaled chiral susceptibility $\chi L^{-\gamma/\nu}$ changes by $\beta \frac{d\chi}{d\beta} L^{-\gamma/\nu}$. This L -dependent change produces a horizontal shift of the intersection point

$$\beta \frac{d(aT_c)}{d\beta} = \beta \frac{d\chi}{d\beta} L^{-\gamma/\nu} [d\chi/d(aT)]^{-1}. \quad (14)$$

The L -independence of this shift is a consistency check of our analysis. The highest accuracy is achieved when $\mu = 0$, for which we determine (on $N_t = 4$ lattices): $aT_c|_{\beta=0} = 1.4021(7)$, $\left. \frac{d}{d\beta} aT_c(\beta) \right|_{\beta=0} = -0.46(1)$.

Several observations are in order. First, aT_c decreases as β increases: this is as it should be, since a decreases. Secondly, this $\mathcal{O}(\beta)$ result can be compared with mean-field predictions [25, 26], see Fig. 5. The agreement is rather good. More importantly, at $\mu = 0$ we can compare with finite- β Hybrid Monte Carlo simulations (at $\mu=0$, these simulations are sign-problem free) performed on $N_t = 2$ and $N_t = 4$ [27–29] lattices with isotropic actions (i.e. $aT = 1/2$ and $1/4$, respectively) and extrapolated to zero quark mass. These data points are marked in black in Fig. 5. We have also computed $aT_c(\mu = 0)$ ourselves, using HMC on anisotropic lattices. As Fig. 5 left shows, our $\mathcal{O}(\beta)$ determination of $aT_c(\mu = 0)$ agrees perfectly with the linear approximation to the HMC determination. But the latter shows significant curvature. To better approximate the exact result, we perform an empirical, exponential extrapolation $aT_c(\mu = 0, \beta)/aT_c(\mu = 0, \beta = 0) \approx \exp(\beta \frac{d}{d\beta} aT_c|_{\beta=0})$.

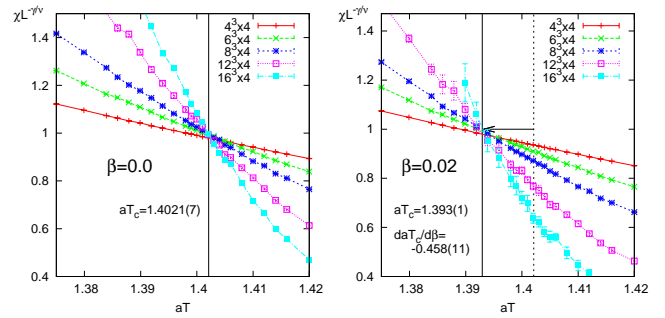


FIG. 4: The $\mu=0$ transition temperature aT_c from finite-size scaling of the chiral susceptibility on $N_t = 4$ lattices. *Left*: $\beta = 0$. *Right*: $\beta = 0.02$. The arrow marks the shift in aT_c .

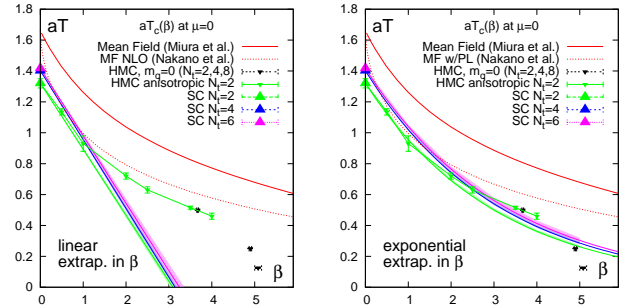


FIG. 5: Phase boundary in $\beta - aT$ plane at $\mu = 0$. *Left*: linear extrapolation. *Right*: exponential extrapolation. The boundary coincides very well with conventional Hybrid Monte Carlo data at large β . Also, the phase boundary is rather similar to the one obtained via a mean field theory prediction without [25] and with Polyakov loop effects [26].

As seen in Fig. 5 right, it turns out that this approximation, which includes a resummation of higher-order β -contributions, follows the exact HMC result up to $\beta \sim 5$ (or $a \sim 0.3$ fm), where the lattice theory is much closer to continuum physics. We have applied the same procedure to determine $aT_c(\beta)$ at non-zero chemical potential. Although the statistical errors increase and the scaling window shrinks, $d(aT_c)/d\beta$ is clearly not as large as when $\mu=0$. In fact, $d(aT_c)/d\beta$ becomes consistent with zero as μ approaches μ_T . The tricritical point and the first order line seem to only weakly depend on β . Thus, $T_c(\mu = 0)/\mu_c(T = 0)$ decreases at $\mathcal{O}(\beta)$ towards its continuum value.

The resulting phase diagram is illustrated in Fig. 6 for $\beta = 0.5, 1.0$ and 1.5 . We show the phase boundary obtained by linear reweighting, based on Eq. (7), compared to the one obtained by exponential extrapolation, which works so well at $\mu = 0$. In both cases, the phase boundary becomes more “rectangular” as one moves away from the strong coupling limit: the second-order transition line becomes “flatter” (less μ -dependent), and the first-order transition line remains almost “vertical”, leaving the tricritical point at the “corner of the rectangle”. From the chiral susceptibility, no clear shift of

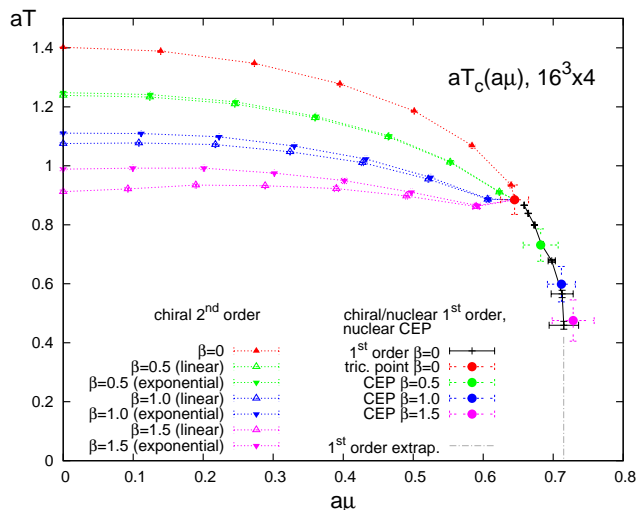


FIG. 6: Phase boundary in the μ - T plane in the strong coupling limit and extrapolated to finite β , comparing linear and exponential extrapolation. We do not observe a shift of the chiral tricritical point. The nuclear critical endpoint (CEP), determined from the reweighted baryon density, moves down along the first order line (extrapolated to $T = 0$ to guide the eye) as β is increased.

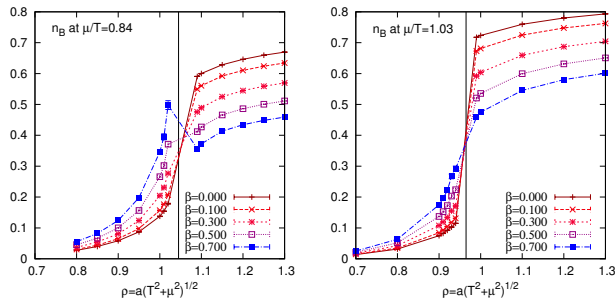


FIG. 7: Reweighted baryon density n_B for $\mu/T > \mu_T/T_T \approx 0.71$, i.e. in the first-order regime. The nuclear transition weakens as β is increased. At some β_c it turns from first order to second order, when the jump in the baryon density vanishes. The larger μ/T , the stronger the first order transition, and the larger β_c . *Left*: μ/T is close to the tricritical point, $\beta_c \approx 0.3$. *Right*: μ/T is larger and $\beta_c \approx 0.7$.

$(a\mu_T, aT_T) = (0.65(2), 0.91(5))$ could be detected; however, from the baryon density n_B , see Fig. 7, we have evidence that the critical endpoint of the nuclear transition, which coincides with the chiral transition at $\beta = 0$, moves along the first order line, to smaller values of T . This is expected: as β increases, the lattice spacing a shrinks, and (aM_B) also, where M_B is the baryon mass. If $(a\mu_c)$ stays approximately constant as we observe, then the nuclear attraction responsible for the difference $(M_B - 3\mu_c(T = 0))$, of about 300 MeV when $\beta = 0$ [6], becomes weaker. The weakening of the as-

sociated first-order transition brings the nuclear critical endpoint point down in temperature. We plan to study $\mathcal{O}(\beta^2)$ corrections next.

We would like to thank K. Miura and A. Ohnishi for helpful discussions.

-
- [1] P. de Forcrand, PoS LAT **2009** (2009) 010
 - [2] M. Fromm, J. Langelage, S. Lottini and O. Philipsen, JHEP **1201** (2012) 042
 - [3] M. Fromm, J. Langelage, S. Lottini, M. Neuman and O. Philipsen, Phys. Rev. Lett. **110** (2013) 122001
 - [4] P. Rossi, U. Wolff, *Nucl. Phys. B* **258** (1984) 105.
 - [5] U. Wolff, *Phys. Lett. B* **153** (1985) 92.
 - [6] P. de Forcrand and M. Fromm, Phys. Rev. Lett. **104** (2010) 112005 [arXiv:0907.1915 [hep-lat]].
 - [7] Y. D. Mercado, C. Gatttringer and A. Schmidt, Phys. Rev. Lett. **111** (2013) 141601 [arXiv:1307.6120 [hep-lat]].
 - [8] K. E. Eriksson, N. Svartholm, B. S. Skagerstam *J. Math. Phys.* **22** (1981) 2276.
 - [9] N. Kawamoto and J. Smit, Nucl. Phys. B **192** (1981) 100.
 - [10] P. H. Damgaard, D. Hochberg and N. Kawamoto, Phys. Lett. B **158** (1985) 239.
 - [11] N. Bilic, F. Karsch, K. Redlich, *Phys. Rev. D* **45** (1992) 3228.
 - [12] N. Bilic, K. Demeterfi, B. Petersson, *Nucl. Phys. B* **377** (1992) 3651.
 - [13] Y. Nishida, *Phys. Rev. D* **69** (2004) 094501.
 - [14] A. Ohnishi, K. Miura, T. Nakano, N. Kawamoto, *PoS (LAT2009)* 160.
 - [15] F. Karsch, K. H. Mütter, *Nucl. Phys. B* **313** (1989) 541.
 - [16] D. H. Adams and S. Chandrasekharan, *Nucl. Phys. B* **662** (2003) 220.
 - [17] W. Unger and P. de Forcrand, PoS LATTICE **2011** (2011) 218
 - [18] S. I. Azakov and E. S. Aliev, Phys. Scripta **38** (1988) 769.
 - [19] M. Creutz, J. Math. Phys. **19** (1978) 2043.
 - [20] Jens Langelage, PhD thesis (2009)
 - [21] P. de Forcrand, S. Kim and W. Unger, JHEP **1302** (2013) 051 [arXiv:1208.2148 [hep-lat]].
 - [22] M. Fromm, J. Langelage, O. Philipsen, P. de Forcrand, W. Unger and K. Miura, PoS LATTICE **2011** (2011) 212 [arXiv:1111.4677 [hep-lat]].
 - [23] T. Hell, K. Kashiwa and W. Weise, Phys. Rev. D **83** (2011) 114008 [arXiv:1104.0572 [hep-ph]].
 - [24] C. Borgs and R. Kotecky, J. Stat. Phys. **61** (1990) 79.
 - [25] K. Miura, T. Z. Nakano, A. Ohnishi and N. Kawamoto, Phys. Rev. D **80** (2009) 074034
 - [26] T. Z. Nakano, K. Miura and A. Ohnishi, Phys. Rev. D **83** (2011) 016014 [arXiv:1009.1518 [hep-lat]].
 - [27] S. A. Gottlieb, W. Liu, D. Toussaint, R. L. Renken and R. L. Sugar, Phys. Rev. D **35** (1987) 3972.
 - [28] R. V. Gavai *et al.* [MT(c) Collaboration], Phys. Lett. B **241** (1990) 567.
 - [29] M. D'Elia and M. -P. Lombardo, Phys. Rev. D **67** (2003) 014505 [hep-lat/0209146].